Kerr effect in Y-configuration double-quantum-dot system

B. Al-Nashy,[1,3] S. M. M. Amin,[1] and Amin H. Al-Khursan[2,*]

[1]*College of Science, University of Basrah, Basrah, Iraq*
[2]*Nassiriya Nanotechnology Research Laboratory (NNRL), Science College, Thi-Qar University, Nassiriya, Iraq*
[3]*Science College, Missan University, Missan, Iraq*
**Corresponding author: ameen_2all@yahoo.com*

Received March 10, 2014; revised May 23, 2014; accepted June 14, 2014;
posted June 26, 2014 (Doc. ID 207814); published July 31, 2014

We have introduced a Y-configuration model from the double-quantum-dot (QD) system to study third-order Kerr nonlinearity based on the density-matrix method. Inhomogeneity in QDs has been included in the calculations of the real (Kerr) and imaginary (absorption) parts of the density matrix, which has not been covered in the earlier Kerr calculations. Our system exhibits high controllability with a single parameter. Giant Kerr dispersion, propagation without distortion, wide electromagnetic-induced transparency, and switching between subluminal to superluminal propagation are obtained by tuning its fields. Controlling and cycling fields can also control the system in addition to the pump field.

OCIS codes: (190.3270) Kerr effect; (160.4236) Nanomaterials.
http://dx.doi.org/10.1364/JOSAB.31.001991

1. INTRODUCTION

Nonlinear quantum optical phenomena based on quantum coherence and interference show considerable importance due to their wide range of applications [1]. These phenomena include electromagnetic-induced transparency (EIT), subluminal and superluminal light propagation, lasing without inversion, and giant Kerr nonlinearity [2]. Many new and important research areas depend on these phenomena, such as quantum information and computing, quantum entanglement, and chemical reaction dynamics [3]. Recently, Kerr nonlinearity has shown interesting applications, such as quantum logic gates, quantum nondemolition measurements, quantum state teleportation, and nonlinear light control. High Kerr nonlinearity at low light powers requires minimization of absorption loss. Conventional devices are incompatible with this requirement [4]. Two- and three-level devices have high resonant absorption and weak nonresonant linearity [5]. Accordingly, EIT is extended, in multilevel systems, to produce a high nonlinearity and suppress linear susceptibility [1,6].

Because of their high nonlinearity, quantum dots (QDs) can be used for obtaining high Kerr dispersion [2,7]. Quantum coherence and interference phenomena in QDs have led to interesting phenomena, such as EIT and superluminal light propagation [8,9]. QD molecules are studied in [9], where both superluminal and subluminal light propagation are demonstrated using interdot tunnel coupling. Enhancement of Kerr nonlinearity with reduced linear and nonlinear absorption via tunnel coupling was also investigated [2], while electric field asymmetry was used [7,10] to enhance Kerr nonlinearity in QD molecules. Linear optical properties for amplification, absorption, and dispersion in double-cascade configurations in the four-level QD system were investigated [11]. In the three-level systems, nonlinear effects cannot be produced because EIT doesn't interact with the probe light. Using multilevel systems, EIT was extended to obtain high nonlinearity and suppress linear susceptibility [1,6]. Accordingly, we have introduced in this work a four-level QD system and then studied the possibility of its manipulation to control its linear and nonlinear absorption and dispersion. Our proposed structure shows a complete control of nonlinear absorption and dispersion by tuning the controlling fields and their phases. This work is organized as follows: In Section 2, the model of Y-type in double QD is proposed; in Section 3, the results are presented and discussed; and in Section 4, this work is concluded.

2. Y-TYPE MODEL IN DOUBLE-QD NANOSTRUCTURES

Consider a four-level Y-type configuration in a QD system. This can be found in a QD molecule with two conduction band levels for each one, as shown in Fig. 1. The inter-sub-band transitions are easily realized experimentally. Sub-band configurations have two subsystems. Sub-bands $|0\rangle$, $|1\rangle$, $|2\rangle$, and $|3\rangle$ form a Λ-type subsystem with a $|0\rangle \to |1\rangle$ transition ($\hbar w_{10}$ energy) that is driven by a weak probe field E_0 (frequency w_0), with Rabi frequency ($\Omega_0 = E_0\mu_{10}/\hbar$): the $|1\rangle \to |2\rangle$ transition ($\hbar w_{21}$ energy) due to the strong cycling field E_1 (frequency w_1), with Rabi frequency ($\Omega_1 = E_1\mu_{21}/\hbar$) and the $|2\rangle \to |3\rangle$ transition ($\hbar w_{32}$ energy) due to the coupling field E_2 (frequency w_2), with Rabi frequency ($\Omega_2 = E_2\mu_{32}/\hbar$). The second subsystem contains $|0\rangle$, $|1\rangle$, and $|3\rangle$ sub-bands and forms a ladder type system with the $|0\rangle \to |1\rangle$ and the $|1\rangle \to |3\rangle$ transitions ($\hbar w_{13}$ energy) due to the strong pump field E_3. The corresponding detunings for these transitions are $\Delta_2 = \omega_2 - \omega_{23}$, $\Delta_m = \omega_m - \omega_{13}$, $\Delta_1 = \omega_1 - \omega_{12}$, and $\Delta_0 = \omega_0 - \omega_{01}$. The two middle levels $|1\rangle$ and $|2\rangle$, the upper level $|3\rangle$, and the ground level $|0\rangle$ form a closed interaction contour. The phases associated with the four coherent fields E_0, E_1, E_2, and E_m are

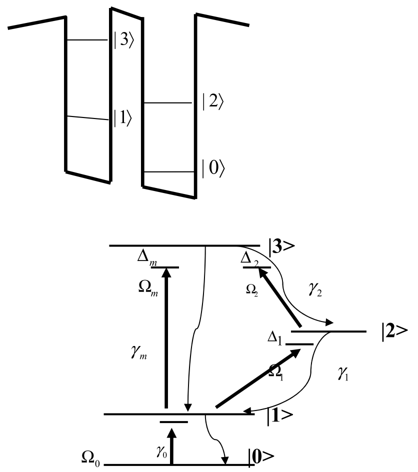

Fig. 1. Schematic energy level diagram of a four-level system in Y-configuration. Here, $\omega_0(\Delta_0)$, $\omega_1(\Delta_1)$, $\omega_2(\Delta_2)$, and $\omega_m(\Delta_m)$ are frequencies (frequency detunings) of probe, cycling, coupling, and pumping fields, respectively.

ϕ_0, ϕ_1, ϕ_2, and ϕ_m, respectively. Driving transitions between double dots by laser fields are examined in a number of works [12,13]. Using the density matrix approach, we can write the following dynamical equations for our system (see Fig. 1):

$$\begin{aligned}
\dot\rho_{00}^{(3)} &= -\gamma_0\rho_{00}^{(3)} + i\Omega_0(\rho_{10}^{(2)} - \rho_{01}^{(2)}),\\
\dot\rho_{11}^{(3)} &= -(\gamma_0\rho_{11}^{(3)} + \gamma_1\rho_{22}^{(3)} + \gamma_m\rho_{33}^{(3)} + i[\Omega_0(\rho_{01}^{(2)} - \rho_{10}^{(2)})\\
&\quad + \Omega_1(\rho_{21}^{(2)} - \rho_{12}^{(2)}) + \Omega_m(\rho_{31}^{(2)} - \rho_{13}^{(2)})],\\
\dot\rho_{22}^{(3)} &= -(\gamma_1\rho_{22}^{(3)} + \gamma_2\rho_{33}^{(3)}) + i[\Omega_1(\rho_{12}^{(2)} - \rho_{21}^{(2)}) + \Omega_2(\rho_{32}^{(2)} - \rho_{23}^{(2)})],\\
\dot\rho_{33}^{(3)} &= -(\gamma_2 + \gamma_m)\rho_{33}^{(3)} + i[\Omega_m(\rho_{13}^{(2)} - \rho_{31}^{(2)}) + \Omega_2(\rho_{23}^{(2)} - \rho_{32}^{(2)})],\\
\dot\rho_{10}^{(3)} &= -(i\Delta_0 + \gamma_0)\rho_{10}^{(3)} + i[\Omega_0(\rho_{00}^{(2)} - \rho_{11}^{(2)}) + \Omega_1\rho_{20}^{(2)}e^{i\varphi} + \Omega_m\rho_{30}^{(2)}],\\
\dot\rho_{20}^{(3)} &= [-i(\Delta_0 + \Delta_1) - (\gamma_0 + \gamma_1)]\rho_{20}^{(3)} + i[\Omega_1\rho_{10}^{(2)}e^{i\varphi}\\
&\quad + \Omega_2\rho_{30}^{(2)} - \Omega_0\rho_{21}^{(3)}e^{i\varphi}],\\
\dot\rho_{30}^{(3)} &= [-i(\Delta_0 + \Delta_m + \Delta_2) - (\gamma_0 + \gamma_2 + \gamma_3)]\rho_{30}^{(3)}\\
&\quad + i[\Omega_m\rho_{10}^{(2)} + \Omega_2\rho_{20}^{(2)} - \Omega_0\rho_{31}^{(2)}],\\
\dot\rho_{12}^{(3)} &= -[i\Delta_0 + i\Delta_1 + \gamma_1]\rho_{12}^{(3)} + i[\Omega_0\rho_{02}^{(2)}e^{i\varphi} + \Omega_1(\rho_{22}^{(2)} - \rho_{11}^{(2)})\\
&\quad + \Omega_m\rho_{32}^{(2)}e^{i\varphi} - \Omega_2\rho_{13}^{(2)}e^{i\varphi}],\\
\dot\rho_{13}^{(3)} &= -(i\Delta_m + i\Delta_2 + \gamma_2 + \gamma_m)\rho_{13}^{(3)} + i[\Omega_m(\rho_{33}^{(2)} - \rho_{11}^{(2)}) + \Omega_0\rho_{03}^{(2)}\\
&\quad + \Omega_1\rho_{23}^{(2)} - \Omega_2\rho_{12}^{(2)}e^{i\varphi}],\\
\dot\rho_{23}^{(3)} &= [-i(\Delta_0 + \Delta_m + \Delta_2) - (\gamma_2 + \gamma_m)]\rho_{23}^{(3)} + i[\Omega_2(\rho_{33}^{(2)} - \rho_{22}^{(2)})\\
&\quad + \Omega_1\rho_{13}^{(2)} - \Omega_m\rho_{21}^{(2)}e^{i\varphi}]. \qquad (1)
\end{aligned}$$

Note that $\phi = \phi_0 + \phi_2 - \phi_1$. γ_i is the total decay constant from sub-band (i). It includes both the lifetime broadening due to longitudinal phonon emission at low temperature and the dephasing broadening, which results from both acoustic phonon scattering and scattering from interface roughness. In QDs, the dephasing broadening is the dominant contribution in contrast to the atomic systems [11]. In this paper, a third-order nonlinear Kerr effect is derived from the probe transition coherence $\rho_{10}^{(3)}$, and then an analytical relation is obtained by taking into account the solution of the system Eq. (1) at steady state. After some (long) mathematical manipulations following the routine way, one can get the following relation:

$$\begin{aligned}
\rho_{10}^{(3)} &= \left[\frac{1}{(i\Delta_0 + \gamma_0)}\right]\left\{\frac{\Omega_0^2}{\gamma_0}d\left[i\Omega_0 - \frac{\Omega_0\Omega_1\rho_{21}e^{2i\varphi}}{a} - \frac{\Omega_2\Omega_m\rho_{20}}{b}\right]\right.\\
&\quad + \frac{\Omega_0^2}{\gamma_0}\left[i\Omega_0 - \frac{\Omega_0\Omega_1\rho_{21}e^{-2i\varphi}}{a} + \frac{\Omega_2\Omega_m\rho_{20}}{b}\right]\\
&\quad \times\left[(i\Delta_0 + \gamma_0) - \frac{\Omega_1^2 e^{-2i\varphi}}{a} - \frac{\Omega_m^2}{b)}\right]^{-1}\\
&\quad + \frac{\Omega_1\Omega_0 e^{2i\varphi}}{a}\left[i\Omega_0 - \frac{\Omega_0\Omega_1\rho_{21}e^{2i\varphi}}{a} + \frac{\Omega_2\Omega_m\rho_{20}}{b}\right]d\\
&\quad - \frac{\Omega_2\Omega_1 e^{i\varphi}}{a}\left[\frac{i(\Omega_m\rho_{10} + \Omega_2\rho_{20})}{b}\right]\\
&\quad + \frac{\Omega_0\Omega_1 e^{2i\varphi}}{a}\left[\frac{i(\Omega_1 - \Omega_0\rho_{20}e^{-i\varphi})}{[-i\Delta_1 + (\gamma_1 + \gamma_0)]}\right]\\
&\quad + \frac{\Omega_m^2}{b}\left[i\Omega_0 - \frac{\Omega_0\Omega_1\rho_{21}e^{2i\varphi}}{a} + \frac{\Omega_2\Omega_m\rho_{20}}{b}\right]d\\
&\quad + \frac{i\Omega_2\Omega_m(\Omega_0\rho_{21}e^{i\varphi} - \Omega_1\rho_{10}e^{i\varphi})}{ba}\\
&\quad \left. + \frac{i\Omega_0\Omega_m(\Omega_m + \Omega_2\rho_{21}e^{i\varphi})}{b[-i(\Delta_m + \Delta_2) + \gamma_2 + \gamma_m]}\right\}, \qquad (2)
\end{aligned}$$

where $a = -i(\Delta_0 + \Delta_1) - (\gamma_0 + \gamma_1)$, $b = -i(\Delta_0 + \Delta_m) - (\gamma_0 + \gamma_2 + \gamma_m)$, and $d = [(i\Delta_0 + \gamma_0) + (\Omega_1^2 e^{2i\varphi}/a) + (\Omega_m^2/b)]^{-1}$.

The nonlinear Kerr susceptibility is then given by

$$\chi^{(3)}(\omega_0) = \int \frac{2N\mu_{01}^4}{3\hbar^3\varepsilon_0\Omega_0^3}\rho_{01}^{(3)}(\omega_0)D(\omega)\mathrm{d}\omega, \qquad (3)$$

where N is the atomic number density in the medium. Our formula differs from all other calculations by including QD inhomogeneity via the convolution over the inhomogeneous density of states, which is given by [14]

$$D(E) = \frac{s^i}{V_{\mathrm{dot}}^{\mathrm{eff}}}\frac{1}{\sqrt{2\pi\sigma^2}}\exp\left(\frac{-(\hbar\omega - E_{\max}^i)^2}{2\sigma^2}\right), \qquad (4)$$

where s^i is the degeneracy number at the QD state ($s^i = 2$) in the quantum disc model used here. σ is the spectral variance of QDs, $V_{\mathrm{dot}}^{\mathrm{eff}}(= h/N_D)$ is the effective volume of QDs, h is the dot height, and N_D is the areal density of QDs. The transition energy at the QD maximum distribution of the ith optical transition is $E_{\max}^i$.

3. RESULTS AND DISCUSSION

The proposed structure (see Fig. 1) is an asymmetric InAs double QD with (10 nm height and 4 nm width) for the left dot and (14 nm height and 2 nm width) for the right dot. Their ground and excited conduction energy sub-bands are (0.8 and 1.07 eV) for the left QD and (0.91 and 1.05 eV) for the right one. This structure can be obtained by the self-assemble growth technique [15]. The ground state (GS) for the left dot is the state $|0\rangle$ of the system, while the GS and the excited state (ES) of the right dot are states $|1\rangle$ and $|2\rangle$, respectively. State $|3\rangle$ is the ES of the left dot. Inclusion of an inhomogeneity is important for susceptibility calculations, which have not been investigated in earlier QD literature that discusses quantum

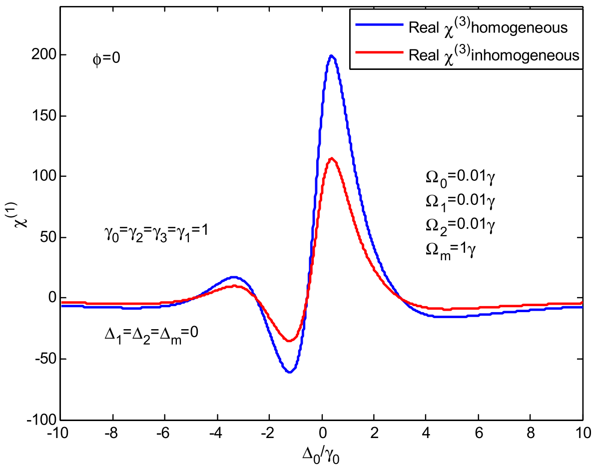

Fig. 2. Comparison between inhomogeneously (red line) and homogeneously broadened (blue line) Kerr dispersion. The detunings are ($\Delta_1 = \Delta_2 = \Delta_m = 0$) while the Rabi field frequencies are ($\Omega_0 = \Omega_1 = \Omega_2 = 0.01\gamma, \Omega_m = 1\gamma$). The phase is zero ($\phi = 0$), while all relaxations are set to 1 meV.

coherence and interference, see, for example, [2,7–10,15]. A uniform ensemble of QD molecules is assumed [12]. Inclusion of inhomogeneity reduces susceptibility; Fig. 2 shows that including inhomogeneous broadening (blue line) reduced Kerr dispersion by about half in comparison with homogeneously broadened Kerr dispersion (red line). This is an expected result where it is demonstrated that the inhomogeneity reduces the optical properties of QD [14]. The comparison in this figure shows that it is critical to include inhomogeneity in the dispersion calculations. Throughout this work, the relaxation from all sub-bands is assumed to be identical ($\gamma_0 = \gamma_1 = \gamma_2 = \gamma_m = 1$ meV). Assumption of identical relaxation is used for simplifying the calculations and can be found in [7] for QD systems, in [16] for atomic systems, and in [17] for quantum well systems. In the following simulated results, inhomogeneity will be included, and they are divided into the following subsections.

A. Detuning Frequency Control

Figure 3 shows the real part of the third-order nonlinear susceptibility versus variation of probe detuning Δ_0 normalized to the relaxation γ_0. The absorption, which is the imaginary part of the linear (third-order) susceptibility, is shown as a red (blue) dashed line for comparison. In Fig. 3(a), the following parameters are considered: ($\Delta_1 = 0$), ($\Delta_2 = \Delta_m = 5\gamma$) probe, pump, cycling, and coupling fields have Rabi frequencies ($\Omega_0 = \Omega_1 = \Omega_2 = 0.01\gamma, \Omega_m = 1.3\gamma$); i.e., only the pump field is strong. Two Kerr peaks and a wide EIT window of about (15γ) are shown. Inside the EIT window, the slope of Kerr dispersion is positive and linear, which results in a large group index of refraction and thus a reduced group velocity [18], i.e., a subluminal light propagation. From the figure, this dispersion occurs at neglected linear and nonlinear absorption (or gain). This result is preferred in applications where the wave travels without distortion (from absorption) or noise (from gain). Around zero probe detuning ($\Delta_0 = 0$), the slope of the Kerr dispersion is negative, with very low linear gain. A high nonlinear gain is obtained collinear with the linear gain, which is added to the linear gain, and then a total gain has a considerable value associated with Kerr dispersion and cannot be neglected. This deteriorates the wave propagation and is undesirable in nonlinear optical applications. Our calculation of nonlinear gain is one of the important features of this study. It is also covered by some other similar works on QDs and other atomic systems (see for example [2,12,16,19]). Figure 3(b) shows the case when the detunings are ($\Delta_1 = \Delta_2 = 0$) and ($\Delta_m = 5\gamma$) with Rabi frequencies ($\Omega_0 = 0.01\gamma$, $\Omega_1 = \Omega_2 = 0.1\gamma, \Omega_m = 0.5\gamma$); i.e., cycling, coupling, and pump fields are strong. Compared with Fig. 3(a), in which only the pump was strong, two high Kerr peaks, which appear at low nonlinear gain points, are increased by ~3 times while the width of the EIT window is reduced by ~3 times. Around zero probe detuning ($\Delta_0 = 0$), a negative Kerr dispersion is shown corresponding to neglected absorption. In Fig. 3(c), the detunings are ($\Delta_1 = \Delta_2 = 5\gamma$) and ($\Delta_m = 0$), while the Rabi frequencies are ($\Omega_0 = 0.01\gamma, \Omega_1 = \Omega_2 = 0.1\gamma, \Omega_m = 1\gamma$), which differs from Fig. 3(a) in that the three controlling fields (pump, cycling, and coupling) are strong and only the pump field is in resonance with its transition energy. A good result is obtained; Kerr peaks increase by ~10 times compared with Fig. 3(a). The two Kerr peaks lie at the EIT window with neglected absorption and a considerable nonlinear gain, but it is about half the value of the Kerr peak. Around zero probe detuning, the Kerr dispersion is also negative. Compared with other works dealing with Kerr in QD and other atomic systems [2,12,16,19], a very giant Kerr value is obtained. In Fig. 3(d), we have set ($\Delta_1 = \Delta_2 = \Delta_m = 5\gamma$) while Rabi frequencies are the same as that in Fig. 3(c). Here, the left Kerr peak is shifted more and the EIT window becomes wider (its width approaches 10γ). In Fig. 3(e), the detunings are ($\Delta_1 = \Delta_2 = 2\gamma, \Delta_m = 0$), and the Rabi frequencies are ($\Omega_0 = 0.01\gamma, \Omega_1 = 0.3\gamma, \Omega_2 = 0.1\gamma, \Omega_m = 1.5\gamma$), which refer to increasing Rabi frequencies of two controlling fields (cycling and pumping). The best result is obtained where the main Kerr peak appearing at the center of the EIT window corresponds to zero linear absorption and reduced nonlinear absorption. Other side peaks appear at the left and right, about ($\pm 7\gamma$) from the main peak with very small linear absorptions and high nonlinear gains. In both Figs. 3(d) and 3(e), the Kerr dispersion is also negative around zero probe detuning. In Fig. 3(f) the detunings are ($\Delta_1 = \Delta_2 = \Delta_m = 5\gamma$), and the Rabi frequencies are ($\Omega_0 = 0.01\gamma, \Omega_1 = \Omega_2 = 0.5\gamma, \Omega_m = 1.5\gamma$), i.e., increasing the three controlling fields, which are not resonant with their corresponding transitions. A positive slope dispersion around zero probe detuning and a wider EIT (~30γ) are obtained. This refers to switching from superluminal [in Figs. 3(a)–3(e)] to subluminal light propagation. Four Kerr dispersion peaks inside the EIT window are obtained, each separated by (~10γ) from their nearest neighbors. Two of them correspond to negligible absorption peaks.

1. Discussion

It is known that detuning the control field varies both the magnitude and position of Kerr dispersion [20]. This is due to the modification of energy states by a laser beam resonant with their energy difference. This results in a scattered photon with distinct coherence and spectral properties that are tuned depending on the laser. Then the bare electronic states are dressed when the Rabi frequency is larger than the spontaneous emission rate [21].

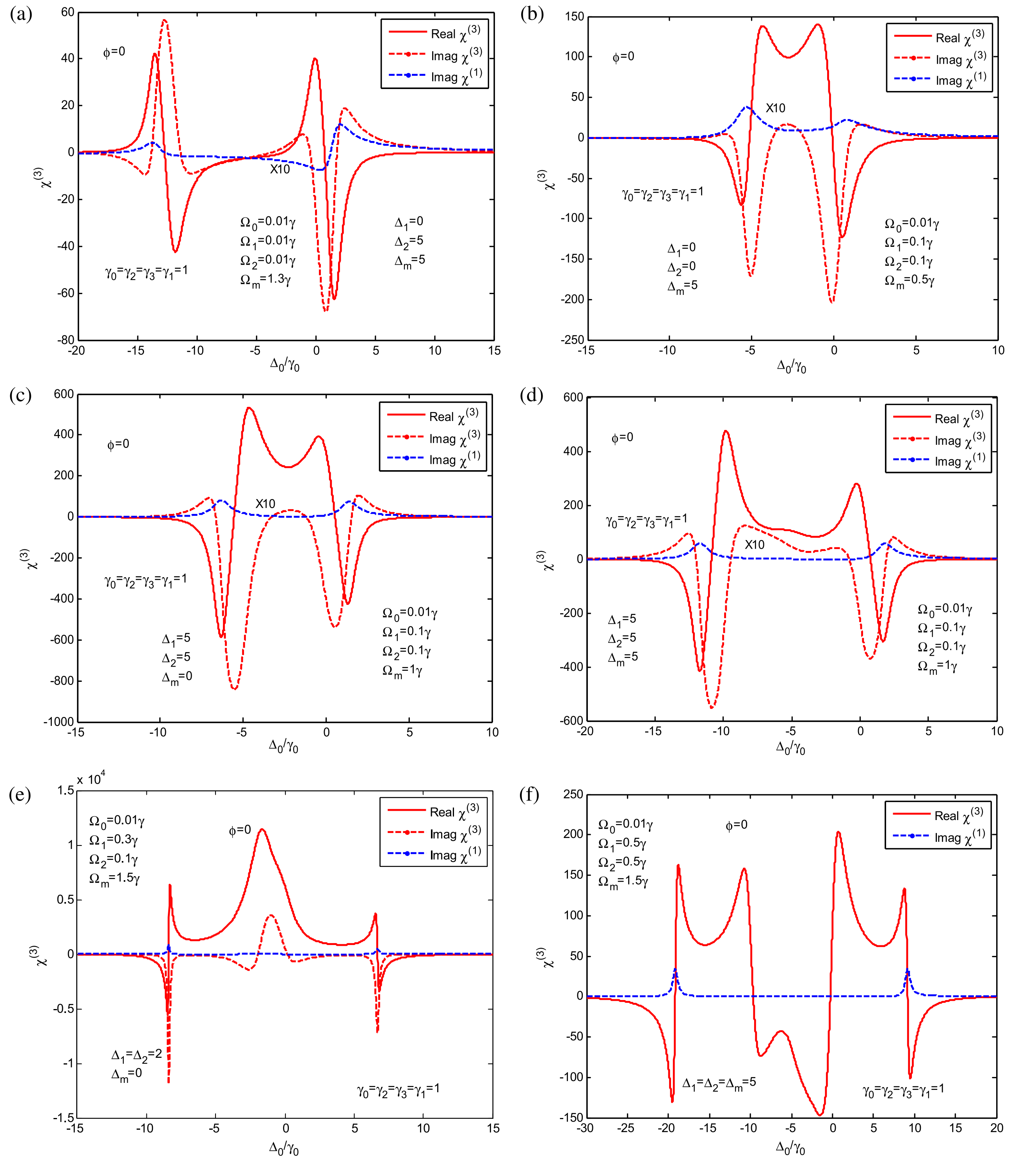

Fig. 3. Third-order susceptibility as a function of probe detuning (Δ_0) normalized to the decay rate (γ_0) for (a) ($\Omega_1 = \Omega_2 = 0.01\gamma, \Omega_m = 1.3\gamma$), ($\Delta_1 = 0$), ($\Delta_2 = \Delta_m = 5\gamma$); (b) ($\Omega_1 = \Omega_2 = 0.1\gamma, \Omega_m = 0.5\gamma$), ($\Delta_1 = \Delta_2 = 0$), and ($\Delta_m = 5\gamma$); and (c) and (d) ($\Omega_0 = 0.01\gamma, \Omega_1 = \Omega_2 = 0.1\gamma, \Omega_m = 1\gamma$), ($\Delta_1 = \Delta_2 = 5\gamma$). In (c), ($\Delta_m = 0$). In (d), ($\Delta_m = 5\gamma$). (e) ($\Omega_0 = 0.01\gamma, \Omega_1 = 0.3\gamma, \Omega_2 = 0.1\gamma, \Omega_m = 1.5\gamma$), ($\Delta_1 = \Delta_2 = 2\gamma, \Delta_m = 0$). In (f), ($\Omega_0 = 0.01\gamma, \Omega_1 = \Omega_2 = 0.5\gamma, \Omega_m = 1.5\gamma$), ($\Delta_1 = \Delta_2 = \Delta_m = 5\gamma$). The phase is zero ($\phi = 0$), while all relaxations are set to 1 meV ($\gamma_0 = \gamma_1 = \gamma_2 = \gamma_3 = \gamma = 1$ meV).

Figure 2 shows that working with resonant fields (zero detunings, EIT center) is important where the Kerr peak is higher than that in Fig. 3(a), which is not at the EIT center, although the pump field is ($\Omega_m = 1\gamma$) in Fig. 2 and ($\Omega_m = 1.3\gamma$) in Fig. 3(a). The destructive quantum interference between the two absorption paths $|0\rangle$, $|1\rangle$, $|3\rangle$ and $|0\rangle$, $|1\rangle$, $|2\rangle$, $|3\rangle$ of two branches of the Y-configuration leads to an EIT window in our QD system. Referring to Fig. 2, an inhomogeneity in QDs due to manufacture imperfection deviates the absorption (or gain) spectrum from the conventional

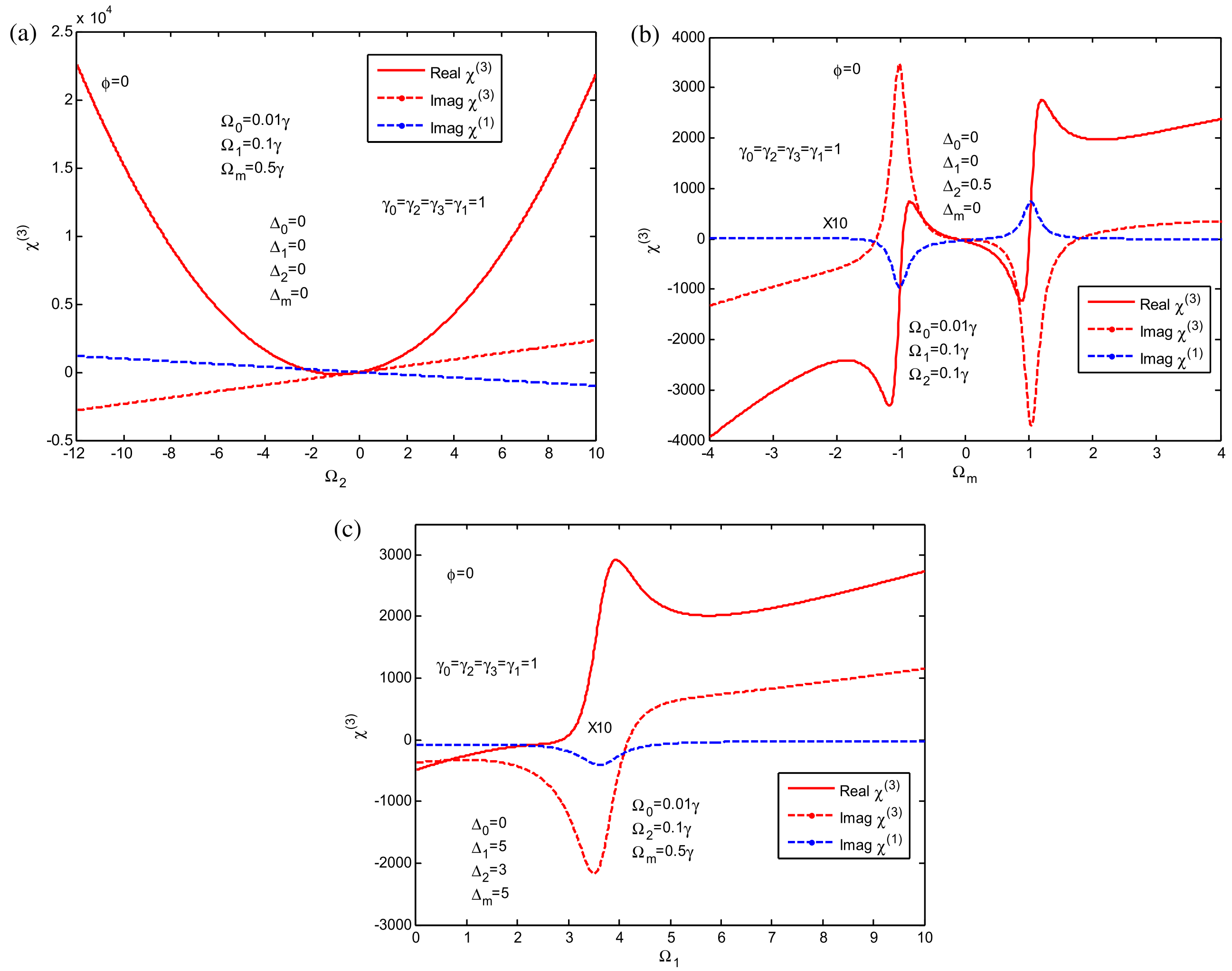

Fig. 4. Third-order susceptibility as a function of different Rabi frequencies in units of (γ): (a) Rabi frequency of coupling with the following parameters: $\Omega_0 = 0.01\gamma$, $\Omega_1 = 0.1\gamma$, $\Omega_m = 0.5\gamma$, and ($\Delta_0 = \Delta_1 = \Delta_2 = \Delta_m = 0$). (b) Rabi frequency of pump $\Omega_0 = 0.01\gamma$, $\Omega_1 = 0.1\gamma$, $\Omega_2 = 0.1\gamma$, and ($\Delta_0 = \Delta_1 = \Delta_m = 0, \Delta_2 = 0.5\gamma$). (c) Rabi frequency of cycling $\Omega_0 = 0.01\gamma$, $\Omega_2 = 0.1\gamma$, $\Omega_m = 0.5\gamma$, and ($\Delta_0 = 0, \Delta_1 = 5\gamma, \Delta_2 = 3\gamma, \Delta_m = 5\gamma$). Other values are $\gamma_0 = \gamma_1 = \gamma_2 = \gamma_3 = \gamma = 1$ meV.

Lorentzian shape. This results in an inhomogeneous shape of absorption spectrum, which is the usual spectrum of QD structure in the absence of a strong pump field. This shape is modulated under strong pump field coupled QD sub-bands [22]. In our Y-configuration QD structure, each pump, cycling, and coupling field coupled with QD sub-bands results in dressed QD states. Since this structure convolutes from four sub-bands in two branches, the pump is not the only controlling field that changes the shape and peak strength of the spectrum. Both cycling and coupling fields work together and control the right branch of the system and finally control all of the system. In Fig. 3(b), increasing the cycling and coupling while reducing the pump to ($\Omega_m = 0.5\gamma$) leads to increasing the Kerr peak to a value higher than that in Figs. 2 and 3(a). This is due to the dark-state results in the Λ-type subsystem ($|3\rangle\leftrightarrow|1\rangle$, $|3\rangle\leftrightarrow|2\rangle$, and $|2\rangle\leftrightarrow|1\rangle$), which is coherently coupled to state $|1\rangle$ via the cycling field and hence double-dark resonance arises. It is known that engineering the width and position of the absorption line is possible [20] by this field (cycling, here) to control the dark state.

Stronger pump, coupling, and cycling fields lead to switching between subluminal and superluminal light propagation, as in Fig. 3(f). Field detunings in our structure control EIT width and, to some extent, peak strength. This is obvious when one compares Figs. 3(c) and 3(d). This is also seen in [20].

B. Rabi Frequency Control

Figure 4(a) shows Kerr dispersion (solid red line) as a function of the Rabi frequency of the coupling field (Ω_2). The linear absorption (blue dashed line) and the nonlinear absorption (red dashed line) are also shown for comparison. The structure is examined at the center of EIT, where all detunings are zero ($\Delta_0 = \Delta_1 = \Delta_m = 0$) (fields are resonant). The Rabi frequencies are ($\Omega_0 = 0.01\gamma, \Omega_1 = 0.1\gamma, \Omega_m = 0.5\gamma$). The important result is obtained at a high coupling field ($\Omega_2 \geq 6\gamma$ and exceeds Ω_m), where a giant Kerr is obtained at neglected linear and nonlinear absorption (or gain), which refers to switching to giant Kerr dispersion by a single controlling parameter (high coupling field) that agrees with the discussion of the above section. Figure 4(b) examines the variation of the susceptibility as a function of the pump field at ($\Delta_2 = 0.5\gamma$), while all other detunings are zero and the fields are ($\Omega_0 = 0.01\gamma, \Omega_1 = \Omega_2 = 0.1\gamma$). High Kerr dispersion is

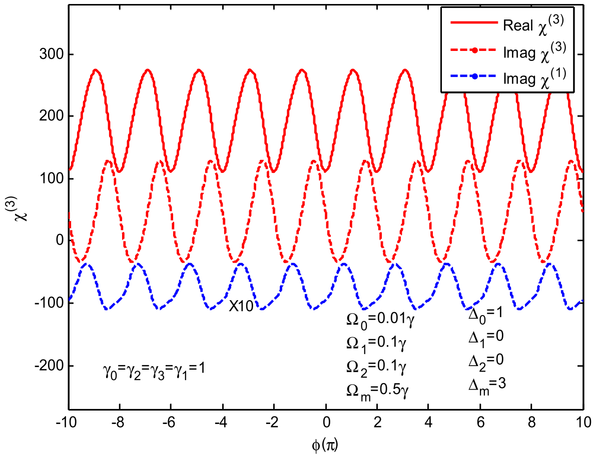

Fig. 5. Real (solid) and imaginary (dashed) nonlinear susceptibility parts as a function of phase for Rabi frequencies $\Omega_0 = 0.01\gamma$, $\Omega_1 = 0.1\gamma$, $\Omega_2 = 0.1\gamma$, and $\Omega_m = 0.5\gamma$. The detunings are ($\Delta_0 = \gamma$, $\Delta_1 = 0, \Delta_2 = 0, \Delta_m = 3\gamma$). Other values are $\gamma_0 = \gamma_1 = \gamma_2 = \gamma_3 = \gamma = 1$ meV.

obtained at ($\Omega_m \geq 2\gamma$) with zero absorption and neglected nonlinear absorption. The effect of the cycling field (Ω_1) is examined in Fig. 4(c) at detunings ($\Delta_0 = 0, \Delta_1 = 5\gamma, \Delta_2 = 3\gamma, \Delta_m = 5\gamma$) and Rabi frequencies ($\Omega_0 = 0.01\gamma, \Omega_1 = 0.1\gamma, \Omega_m = 0.5\gamma$). The important result is obtained at ($\Omega_1 = 4\gamma$), where a high Kerr is obtained at neglected linear and nonlinear absorption. This is important for pulse propagation to overcome the pulse distortion inside the medium with high absorption, while a gain may add noise to the pulse through the amplifying medium.

C. Phase Control

Figure 5(a) shows the Kerr dispersion (red solid line) as a function of phase (ϕ). Both linear (blue dashed line) and nonlinear susceptibility (red dashed line) are shown for comparison. The detunings are set to ($\Delta_0 = \gamma, \Delta_1 = \Delta_2 = 0, \Delta_m = 3\gamma$) while the fields are ($\Omega_0 = 0.01\gamma, \Omega_1 = \Omega_2 = 0.1\gamma, \Omega_m = 0.5\gamma$). High peaks of Kerr dispersion are obtained at low linear absorption and low nonlinear gain. This is important in the application of slow light levels where the dispersion rises above the absorption, as shown here. Figure 5 is another example of controlling our structure by a single parameter (phase).

4. CONCLUSIONS

A model for the Kerr effect in a Y-configuration QD system is proposed using the density-matrix formalism. Inhomogeneity in QDs is shown to be critical in the dispersion Kerr calculations in QD systems. Using the controllable fields, detunings, and phases, switching between subluminal and superluminal light propagations, distortionless propagation, wide EIT, and a giant Kerr nonlinearity is obtained.

REFERENCES

1. M. D. Lukin, S. F. Yelin, M. Fleischhauer, and M. O. Scully, "Quantum interference effects induced by interacting dark resonances," Phys. Rev. A **60**, 3225–3228 (1999).
2. S. H. Asadpour, M. Sahrai, R. Sadighi-Bonabi, A. Soltani, and H. Mahrami, "Enhancement of Kerr nonlinearity at long wavelength in a quantum dot nanostructure," Physica E **43**, 1759–1762 (2011).
3. Y. Niu, S. Gong, R. Li, and S. Jin, "Creation of atomic coherent superposition states via the technique of stimulated Raman adiabatic passage using a L-type system with a manifold of levels," Phys. Rev. A **70**, 023805 (2004).
4. H. Kang and Y. Zhu, "Observation of large Kerr nonlinearity at low light intensities," Phys. Rev. Lett. **91**, 093601 (2003).
5. J. Kou, R. G. Wan, Z. H. Kang, H. H. Wang, L. Jiang, X. J. Zhang, Y. Jiang, and J. Y. Gao, "EIT-assisted large cross-Kerr nonlinearity in a four-level inverted-Y atomic system," J. Opt. Soc. Am. B **27**, 2035–2039 (2010).
6. A. B. Matsko, I. Novikova, G. R. Welch, and M. S. Zubairy, "Enhancement of Kerr nonlinearity by multiphoton coherence," Opt. Lett. **28**, 96–98 (2003).
7. Y. Jiang and K. Zhu, "Controlling Kerr nonlinearity with electric fields in asymmetric double quantum-dots," arXiv:0801.3726v1 (2008).
8. M. Mahmoudi and M. Sahrai, "Absorption-free superluminal light propagation in a quantum-dot molecule," Physica E **41**, 1772–1778 (2009).
9. A. H. Al-Khursan, M. K. Al-Khakani, and K. H. Al-Mossawi, "Third-order non-linear susceptibility in a three-level QD system," Photon. Nanostr. Fundam. Appl. **7**, 153–160 (2009).
10. Y. She, X. Zheng, D. Wang, and W. Zhang, "Controllable double tunneling induced transparency and solitons formation in a quantum dot molecule," Opt. Express **21**, 17392–17403 (2013).
11. X. Hao, J. Wu, and Y. Wang, "Steady-state absorption–dispersion properties and four wave mixing process in a quantum dot nanostructure," J. Opt. Soc. Am. B **29**, 420–428 (2012).
12. A. Vafafard, S. Goharshenasan, N. Nozari, and A. Mohmoudi, "Phase-dependent optical bistability in the quantum dot nanostructure molecules via inter-dot tunnelling," J. Lumin. **134**, 900–905 (2013).
13. M. Sahrai, M. Reza Mehmannavaz, and H. Sattari, "Optically controllable switch for light propagation based on triple coupled quantum dots," Appl. Opt. **53**, 2375–2383 (2014).
14. J. Kim and S. L. Chuang, "Theoretical and experimental study of optical gain, refractive index change, and linewidth enhancement factor of p-doped quantum-dot lasers," IEEE J. Quantum Electron. **42**, 942–952 (2006).
15. G. G. Tarasov, Z. Ya. Zhuchenko, M. P. Lisitsa, Yu. I. Mazur, Zh. M. Wang, G. J. Salamo, T. Warming, D. Bimberg, and H. Kissel, "Optical detection of asymmetric quantum-dot molecules in double-layer InAs/GaAs structures," Semiconductors **40**, 79–83 (2006).
16. H. R. Hamedi, S. H. Asadpour, and M. Sahrai, "Giant Kerr nonlinearity in a four-level atomic medium," Optik **124**, 366–370 (2013).
17. A. Joshi, "Phase-dependent electromagnetically induced transparency and its dispersion properties in a four-level quantum well system," Phys. Rev. B **79**, 115315 (2009).
18. C. J. Chang-Hasnain, P.-C. Ku, J. Kim, and S.-L. Chuang, "Variable optical buffer using slow light in semiconductor nanostructures," Proc. IEEE **91**, 1884–1897 (2003).
19. X. Hao, W. X. Yang, X. Lua, J. Liu, P. Huang, C. Ding, and X. Yang, "Polarization qubit phase gate in a coupled quantum-well nanostructure," Phys. Lett. A **372**, 7081–7085 (2008).
20. Y. Niu, S. Gong, R. Li, Z. Xu, and X. Liang, "Giant Kerr nonlinearity induced by interacting dark resonances," Opt. Lett. **30**, 3371–3373 (2005).
21. A. N. Vamivakas, Y. Zhao, C.-Y. Lu, and M. Atature, "Spin resolved quantum dot resonance fluorescence," Nat. Phys. **5**, 198–202 (2009).
22. X. Xu, B. Sun, P. R. Berman, D. G. Steel, A. S. Bracker, D. Gammon, and L. J. Sham, "Coherent optical spectroscopy of a strongly driven quantum dot," Science **317**, 929–932 (2007).